SCIENTIFIC REPORTS

OPEN

SUBJECT AREAS:
ULTRACOLD GASES
ATOMIC AND MOLECULAR COLLISION PROCESSES

Received
15 January 2014

Accepted
28 April 2014

Published
27 May 2014

Correspondence and requests for materials should be addressed to W.-M.L. (wliu@iphy.ac.cn)

The confinement induced resonance in spin-orbit coupled cold atoms with Raman coupling

Yi-Cai Zhang, Shu-Wei Song & Wu-Ming Liu

Beijing National Laboratory for Condensed Matter Physics, Institute of Physics, Chinese Academy of Sciences, Beijing 100190, China.

The confinement induced resonance provides an indispensable tool for the realization of the low-dimensional strongly interacting quantum system. Here, we investigate the confinement induced resonance in spin-orbit coupled cold atoms with Raman coupling. We find that the quasi-bound levels induced by the spin-orbit coupling and Raman coupling result in the Feshbach-type resonances. For sufficiently large Raman coupling, the bound states in one dimension exist only for sufficiently strong attractive interaction. Furthermore, the bound states in quasi-one dimension exist only for sufficient large ratio of the length scale of confinement to three dimensional s-wave scattering length. The Raman coupling substantially changes the confinement-induced resonance position. We give a proposal to realize confinement induced resonance through increasing Raman coupling strength in experiments.

The experimental realizations of synthetic gauge field and the spin-orbit coupling (SOC) in neutral cold atoms provide a new arena to explore the exotic effects in cold atomic physics. For example, the SOC could bring about nontrivial ground states in Bose-Einstein Condensate (BEC), such as vortex or vortex lattice states, plane wave phase, standing wave phase[1–10]. The prominent effect induced by the SOC in fermions is that the SOC could enhance the low energy density of states, which results in the formation of two-body bound states and enhancement of the pairing gap[11,12]. In polarized fermion gas, the spin-orbit coupling modifies the finite temperature phase diagram[13]. The exotic dynamic effect, e.g. *Zitterbewegung* oscillation, appears in the spin-orbit coupled cold atomic gas[14,15]. In the presence of SOC, the two-body scattering properties in three dimension have been investigated. It is shown that the SOC usually results in the mixed-partial-wave scattering[16]. For the low-energy scattering, the short range behaviors of wave function in three dimension can be modified by the SOC[17–19]. The two-body scattering properties in qusi-two-dimensional confinement with pure Rashba spin-orbit coupling are investigated[20].

For the low-dimensional quantum gas, the two-body scattering properties can be affected greatly by the external confinement potential. For example, when the s-wave scattering length is comparable to the transverse confinement length ($a_s/a_\perp = 1/C$ with $C = -\zeta(1/2) \approx 1.46$), there exists a resonance, wherein the one-dimensional effective interaction constant diverges[21,22]. The similar scenario of the confinement induced resonance (CIR) also occurs in the quasi-two-dimensional case[23,24]. The confinement induced resonance has been observed through producing confinement induced molecules in quasi-one -dimensional Fermi gas[25]. It is also found experimentally that a single resonance splits into two resonances by introducing the anisotropic confinements[26]. The transversally anisotropic confinement alters the position of resonance by tuning the anisotropic ratio[27,28]. The confinement induced resonance which can be used to tune the interaction between atoms, provides a crucial ingredient to realize the strong interacting low-dimensional systems, such as Tonks-Girardeau gas[29,30] and possible Tomonaga-Luttinger liquid[31,32].

Some novel quantum states, for example, topological superfluidity, Majorana edge states or non-Abelian anyons could emerge in the low-dimension spin-orbit coupled quantum gas with Zeeman field[33–35]. In experiments, an effective Zeeman field in spin-orbit coupled atomic gas can be produced by two-photon Raman coupling[36–41]. The Raman coupling strength corresponds to the effective Zeeman field strength. The combination of the Raman coupling and SOC plays an essential role in the formation of the above novel quantum states. The effects induced by the Raman coupling and SOC are usually considered within BCS (Bardeen-Cooper-Schrieffer) mean-field framework[42,43]. It is known that the two-body interaction properties provide basis for understanding the many-body system. The studies on the effects of the Raman coupling on two-body problem may give some

insight into exotic quantum states. In addition, the confinement induced resonance provides the indispensable tool for the realization of the low-dimensional strongly interacting quantum gas. Furthermore, how the Raman coupling and SOC affect confinement induced resonance is an inevitable question to clarify. In the present paper, we try to address the above questions by studying the two-body scattering problem in one dimension and the confinement induced resonance in the presence of the Raman coupling and SOC.

Results

The two-body scattering in the presence of spin-orbit coupling and Raman coupling. We consider the Hamiltonian of spin-orbit coupled cold atoms with Raman coupling

$$\begin{aligned} H &= H_K + H_0 + V(x), \\ H_K &= \frac{K^2}{4m} + \frac{\gamma K}{2m}\left(\sigma_2^x + \sigma_1^x\right), \\ H_0 &= \frac{k^2}{m} + \frac{\gamma k}{m}\left(\sigma_2^x - \sigma_1^x\right) + \frac{\Omega}{2}\left(\sigma_2^z + \sigma_1^z\right), \end{aligned} \tag{1}$$

where the H_K is the Hamiltonian in center of mass coordinate of two atoms, H_0 is the free Hamiltonian in relative coordinate. K and k are the total momentum and relative momentum of two atoms along x direction, respectively. σ^x and σ^z are the spin Pauli matrix and $V(x)$ is the interaction between two particles. γ denotes the SOC strength and Ω is the two-photon Raman coupling strength between two Zeeman sublevels in experiment. The SOC strength is determined by $\gamma = 2\pi\hbar sin(\theta/2)/\lambda$, where λ is the Raman laser wave length, m is the mass of atom, θ is the angle between two Raman beams. The above Hamiltonian is realized experimentally in fermion atomic gas of ^{40}K[38]. The above spin-orbit coupling is the mixture of equal Rashba and Dresselhaus type. Here, we choose the x axial direction as the direction of momentums. For simplicity, in the whole manuscript we denote K and k as the total and relative momentums, respectively, rather than K_x and k_x. The above Hamiltonian can be obtained from the Hamiltonian in Ref. 38 by applying a rotation in spin space ($\sigma^x \to \sigma^z$, $\sigma^y \to \sigma^y$ and $\sigma^z \to -\sigma^x$). We take the natural units $m = 1$, $\hbar = 1$ and $\gamma = 1$ in this section.

From Eq. (1), we know that the motion of center of mass is coupled to the relative motion through spins. In the following, we focus on the subspace of Hamiltonian with $K = 0$ (the effects of the non-zero total momentum are also discussed). In the spin basis $\left[|s\rangle = (\uparrow\downarrow - \downarrow\uparrow)/\sqrt{2}, |t_1\rangle = \uparrow\uparrow, |t_2\rangle = \downarrow\downarrow, |t_3\rangle = (\uparrow\downarrow + \downarrow\uparrow)/\sqrt{2}\right]$, the Raman coupling and SOC are transformed into $M = 2\gamma\left[k/\sqrt{2}|s\rangle(\langle t_1| - \langle t_2|) + h.c + \Omega/2\gamma(|t_1\rangle\langle t_1| - |t_2\rangle\langle t_2|)\right]$. The interaction between cold atoms can be modeled by zero-range pseudo potential. Furthermore, we consider two identical spin-1/2 fermions. Hence, only the s-wave interaction in the singlet channel has contribution to two-body scattering. Therefore, the interaction matrix between two atoms takes the form as $V(x) = |s\rangle\langle s| \otimes g_{1D}\delta(x)$, where g_{1D} is one-dimensional interaction constant. From the matrix V and M, we know that the spin channel $|t_3\rangle$ is decoupled from other channels and not affected by the interaction. Thus, the spin channel $|t_3\rangle$ is dropped in the following, and the Hamiltonian H_0 is reduced to a 3×3 matrix. After diagnalizing H_0, the eigenenerges are obtained as $E_1(k) = k^2 + 2\gamma\sqrt{k^2 + (\Omega/2\gamma)^2}$, $E_2(k) = k^2$, $E_3(k) = k^2 - 2\gamma\sqrt{k^2 + (\Omega/2\gamma)^2}$ (see the panel (**a**) of Fig. 1), respectively. When the total momentum $K \neq 0$, the spin channel $|t_3\rangle$ will couple with other states. Then, the H_0 is a 4×4 matrix and there are four continuous energy branches [see the panel (**b**) of Fig. 1].

The scattering problem can be solved through the Lipmann-Shwindger equation (for details see **Metholds**). The scattering with Raman coupling and SOC is intrinsically multi-channel scattering problem[44,45]. There exist different scattering thresholds for different energy branches. When the incident energy crosses the thresholds, some scattering channels are opened or closed. In certain scattering energy interval, there may exist several scattering channels scattering each other (see Fig. 1). The scattering amplitudes $f_{m,n}$ (reflection amplitudes) make up a matrix of rank 1, where the subscript n (m) denotes the specific incident (reflecting) channel with a specific energy ϵ. A single total amplitude f is obtained by diagnalizing the scattering matrix in every energy interval.

It is known that in the usual case without Raman coupling and SOC, the reflection coefficient approaches one (total reflection) as the incident energy approaches the scattering threshold of $\epsilon_{th} = 0$. For a fixed incident energy $\epsilon > 0$, the reflection also approaches total reflection as the interaction g_{1D} approaches infinity. For attractive interaction $g_{1D} < 0$, there always exists a bound state below the scattering threshold.

In Figs. 2 and 3, we calculate the reflection coefficient ($|f|^2$) from the obtained scattering amplitude f. We can see that, compared with the usual case, the Raman coupling and SOC cause fundamental changes in the behaviors of the scattering amplitude at low energy. **First of all**, there exist scattering resonances in the parameter space because there exist quasi-bound states between the energy branches. The interaction matrix V can be rewritten in terms of the eigen-basis of H_0. In addition to the interaction in the respective eigen-basis channel (diagonal part), there are also non-diagonal part coupling to different eigen-basis. The upper energy branches could support bound states near the incident energy. In addition, the bound states are coupled to the scattering states due to the non-diagonal interaction term. Hence, it results in a Feshbach-type resonance scattering[46–48]. **Secondly**, when the collision energy approaches the lowest threshold, the reflection coefficient does not approach 1. So the incident wave could not be totally reflected in the presence of SOC and Raman coupling. **Thirdly**, the reflection may vanish under certain conditions. As shown in Fig. 2 and panel (**a**) of Fig. 3, as the incident energy approaches the threshold of $\epsilon = 0$ from below, the scattering amplitude becomes zero no matter how large the interaction is. This is because when the incident energy approaches the threshold of zero energy from below ($\epsilon \to 0_-$), the middle energy branch E_2 contributes a infinitely large real number $\left(G_{11}(0) \sim \frac{1}{2\pi}\int_{\infty}^{\infty} dk\left[\frac{1}{\epsilon - E_2 + i\eta}\frac{(\Omega/2)^2}{k^2 + (\Omega/2)^2}\right] \approx -1/2\sqrt{-\epsilon}\right)$ to the denominator of the scattering amplitude (see Eq. (4) in **Metholds**). **Next**, as the interaction g_{1D} approaches infinity, contrary to the usual case, the reflection needs not mean a total reflection. Due to the coupling between singlet and triplet channels caused by the SOC, the incident wave can tunnel through other channels, even the interaction strength is very strong in singlet channel. A similar scenario also appears in impurity scattering problems of multi-component coupled system[49].

Finally, the large Raman coupling changes the conditions of the existence of bound states. When the Raman coupling satisfies $0 < \Omega \leq 2\gamma$, there always exists a bound state below the lowest threshold for attractive interaction $g_{1D} < 0$ as the usual case. However, if $\Omega > 2\gamma > 0$, there exists a bound state only when the attractive interaction is strong enough. This is because when the energy approaches the lowest threshold ($\epsilon \to -\Omega$), all the energy branches contribute a finite part $\left(G_{11}(0) = \frac{1}{2\pi}\int_{\infty}^{\infty} dk\left[\frac{1}{\epsilon - E_2 + i\eta}\frac{(\Omega/2)^2}{k^2 + (\Omega/2)^2} + \frac{1}{\epsilon + i\eta - E_1}\frac{k^2}{k^2 + (\Omega/2)^2} + \frac{1}{\epsilon + i\eta - E_3}\frac{k^2}{k^2 + (\Omega/2)^2}\right]\right)$ to the denominator of the scattering amplitude (see Eq. (4) in **Metholds**), rather than an infinitely large number as that in usual case without Raman coupling and SOC. The existence of the bound states is directly related to the density of states near the lowest scattering threshold. It is known that, in the usual case,

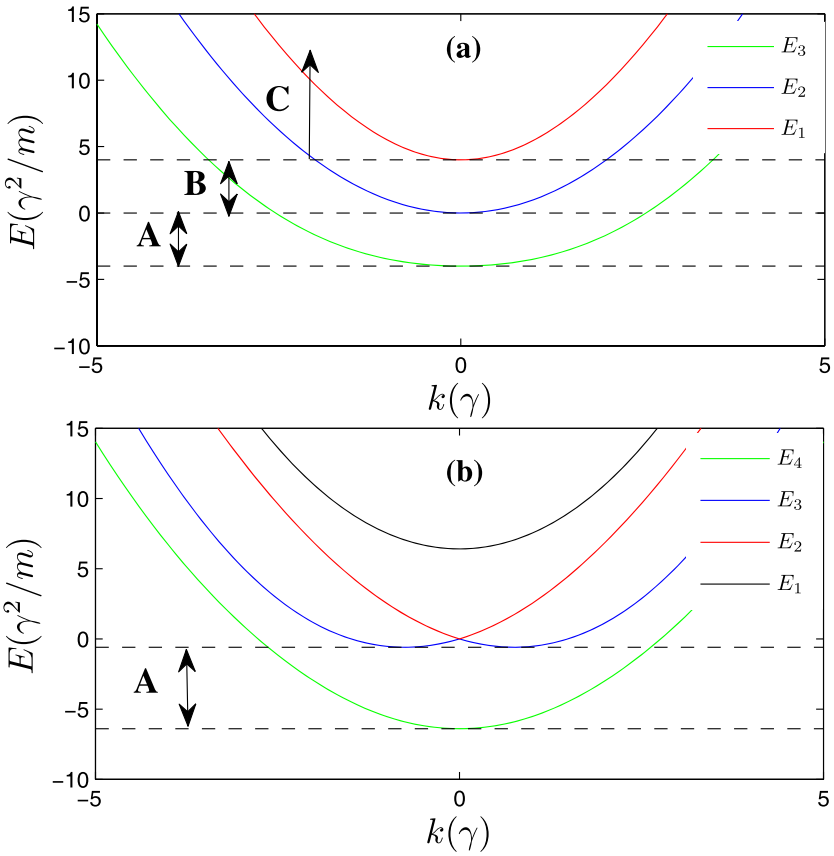

Figure 1 | The energy spectrum of the relative motion (the Raman parameter $\Omega = 4\gamma^2/m$). (a): There are three energy branches ($K = 0$), the highest E_1, the middle one E_2 and the lowest branches E_3. When the Raman coupling is weak ($\Omega \leq 2\gamma$), there exist two minimums on the lowest energy branch E_3 (not shown in the Figure). When the Raman coupling is strong enough ($\Omega > 2\gamma$), the lowest threshold is $-\Omega$ locating at the zero momentum of the lowest energy branch E_3. The A, B and C label three different scattering energy intervals $[-4, 0]$, $[0, 4]$ and $[4, \infty)$, respectively. The numbers of the scattering channels in different energy intervals are different. (b): Due to non-vanishing total momentum ($K = 5\gamma$), the spin-state $|\uparrow\downarrow + \downarrow\uparrow\rangle$ would couple with other spin states. So there would be four continuous energy branches.

the density of states in one dimension near the scattering threshold ($\epsilon_{th} = 0$) behaves like $\sim \frac{1}{\sqrt{\epsilon}}$. There always exists a bound state bellow the scattering threshold ϵ_{th} as long as the interacting ($g_{1D} < 0$) is attractive (no matter how weak it is). When the Raman coupling is weak ($\Omega \leq 2\gamma$), the lowest energy branch has two minimums occurring at non-zero momentums. The density of states near the minimums also looks like $\propto \frac{1}{\sqrt{\epsilon}}$ (the ϵ is measured with respect to the minimum of the continuous spectrum).

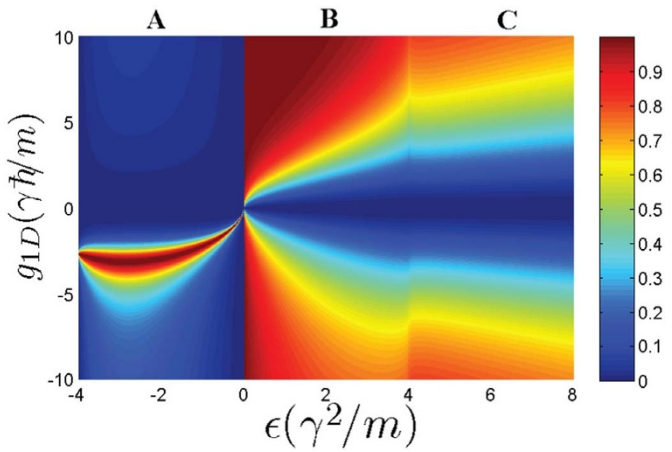

Figure 2 | The reflection coefficient $|f|^2$ as a function of the interaction g_{1D} and the scattering energy ϵ when $\Omega = 4\gamma^2/m$ ($K = 0$). f is the scattering (reflection) amplitude in one dimension. The corresponding three scattering energy intervals in panel (a) of Fig. 1 are also labeled here.

Then the conditions of existence of bound states are the same as the usual case. However, if the Raman coupling is strong enough ($\Omega > 2\gamma$), the lowest energy branch has only one minimum locating at the zero momentum (see the Fig. 1). Intuitively thinking, the density of states should be proportional to $\frac{1}{\sqrt{\epsilon}}$. However, at the zero momentum, we can see that the spin-orbit coupling does not play role at all in the energy spectrum (see Eq. (1)). The lowest point should correspond to the spin-triplet state, rather than the singlet state. Furthermore, we consider the interaction occurring only in the singlet channel. So the effective density of states near the lowest threshold which could contribute to the formation of bound state is very low. For example, there exists a suppression factor $\left(\sim \frac{k^2}{k^2 + (\Omega/2)^2}\right)$ in the denominator of the scattering amplitude (see Eq. (4) in **Methods**). The effective density of states near the lowest scattering threshold behaves like $\sqrt{\epsilon}$ approaching to zero as $\epsilon \to 0$ (the ϵ is measured with respect to the lowest scattering threshold), rather than like $1/\sqrt{\epsilon}$ blowing up. So, in this case, there exist bound states only when the interaction is strong enough. In the following, we will see that the modifications of effective density of states near the lowest threshold also have significant impacts on the existence of the bound states of quasi-one-dimensional system.

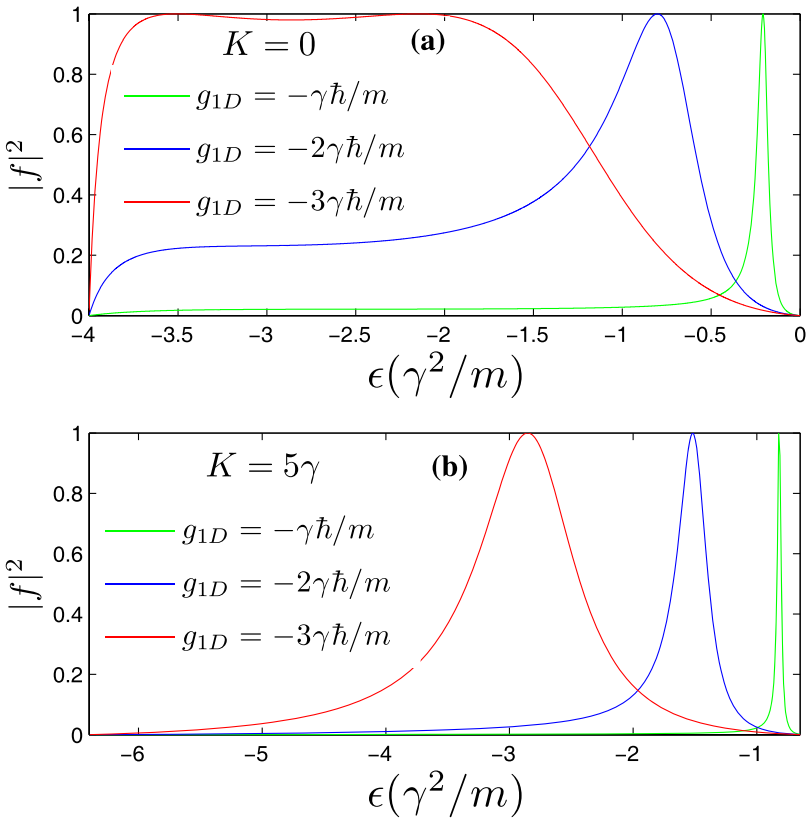

Figure 3 | The reflection coefficients in the energy interval A of Fig. 1. (a): the refection coefficient corresponding to $K = 0$. (b): the refection coefficient corresponding to $K = 5\gamma$. The Feshbach resonance peaks correspond to the quasi-bound states embedded between the continuous energy branches. The resonance position and width vary with the increase of the interaction strength. We can see that when the incident energy ϵ approaches the threshold of the middle branch E_2, the reflection vanishes. When the incident energy ϵ approaches the lowest threshold the reflections are not total reflections.

The modifications of scattering properties are robust even for non-zero total momentum $K \neq 0$ (see the panel (**b**) of Fig. 3). However, the position and width of Feshbach Resonance are usually modified by the non-zero total momentum. Fig. 4 shows the energy of bound states (with respect to the lowest scattering threshold) for attractive interaction ($g_{1D} < 0$) in the pure one-dimensional system. We can see that, with increase of total momentum K, the critical interaction magnitude $|g_{1D}|$ where the bound states begin to appear near the lowest threshold becomes larger and larger. From the above discussion, we know that for stronger Raman coupling Ω, the required interaction strength $|g_{1D}|$ should be stronger in order to form a bound state. So the effects of the $K \neq 0$ is similar to that of increasing Raman coupling. In the next section, we will see the conclusion that the increase of total momentum K amounts to increasing the Raman coupling Ω is also valid for the quasi-one-dimensional system.

The confinement induced resonance. The one-dimensional effective interaction constant is derived through investigating two-body problem of three dimension with confinement. The Raman coupling and SOC may change the condition of confinement induced resonance. After separating the motion of center of mass, the Hamiltonian with confinement can be written as

$$\begin{aligned} H_r &= H_0 + H_\perp + V(r), \\ H_\perp &= -\frac{\hbar^2}{2\mu}\left(\partial_y^2 + \partial_z^2\right) + \frac{\mu\omega_\perp^2}{2}\left(y^2 + z^2\right), \end{aligned} \tag{2}$$

where H_0 is the free Hamiltonian of relative coordinate along x direction as above section, $H_\perp$ is transverse confinement, $V(r) = |s\rangle\langle s| \otimes g_{3D}\delta(\overrightarrow{r})\partial_r(r\cdot)$ is the three dimensional s-wave psuedo-potential interaction between atoms[50,51]. $g_{3D} = 4p\hbar^2 a_s/m$ and $\omega_\perp$ are the three dimensional interaction constant and frequency of confinement trap, respectively. a_s and $\mu = m/2$ are the s-wave scattering length and the reduced mass of two atoms, respectively. In this section, we take natural units as $m = 1$, $\hbar = 1$ and $\omega_\perp = 1$.

The one-dimensional effective interaction constant g_{1D} can be obtained in terms of the three dimensional s-wave scattering length a_s (see **Methods**),

$$g_{1D} = \frac{2\hbar^2 a_s}{\mu a_\perp^2}\frac{1}{1-(C_1+C_2)a_s/a_\perp}, \tag{3}$$

with

$$\begin{aligned} C_1 &= \frac{-1}{\sqrt{\pi}}\int_0^\infty dt\left[\frac{e^{\epsilon t/2}}{(e^t-1)/\sqrt{t}} - \frac{1}{t^{3/2}}\right], \\ C_2 &= \frac{-1}{\sqrt{2\pi}}\int_0^\infty dt\frac{e^{\epsilon t/2}}{e^t-1} \\ &\quad \int_{-\infty}^\infty dk\frac{e^{-k^2t/2}k^2\left[\cosh\left(\gamma t\sqrt{k^2+(\Omega/2\gamma)^2}\right)-1\right]}{k^2+(\Omega/2\gamma)^2} \end{aligned}$$

The above equation gives the connection between the one-dimensional effective interaction constant g_{1D} and the three dimensional s-wave scattering length. When the SOC vanishes ($\gamma = 0$), C_2 becomes zero. Furthermore, if the scattering energy $\epsilon \to 0$, the constant $C_1 = C$

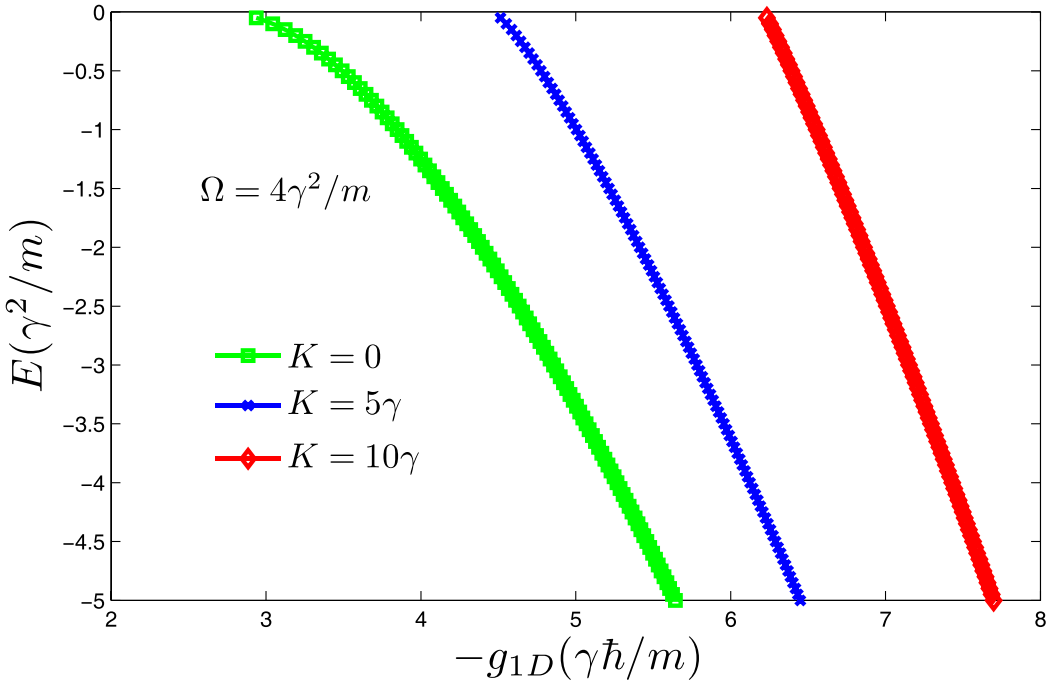

Figure 4 | The energy of bound states for attractive interaction ($g_{1D} < 0$) in one dimension From the Fig. 4, we can see the energy of bound states is getting lower and lower with increase the interaction magnitude $|g_{1D}|$. The critical interaction magnitude is large for large total momentum K. So the effects of K are very similar to that of increasing Raman coupling.

$= -\zeta(1/2) \approx 1.46$, the resonance condition is reduced to Olshanii's result[21].

From panel (**a**) of Fig. 5, we can find that, with the increase of the Raman coupling, the resonance position $a_s/a_\perp$ is getting smaller. In addition, the resonance position inclines to be independent of SOC strength for sufficiently large Raman coupling ($\Omega \gg 1$). In fact, the resonance position $a_s \Big/ a_\perp \sim 1 \Big/ \sqrt{2\Omega}$ can be arbitrarily small by increasing the Raman parameter Ω for fixed SOC parameter ($\gamma \sim 1$). It can be shown that, for a fixed spin-orbit coupling ($\gamma = 1$), $C_1 \sim \sqrt{2\Omega}$ diverges and C_2 is bounded as $\Omega \to \infty$. When the condition of confinement induced resonance is satisfied, from Eq.(3), the resonance position $a_s \Big/ a_\perp = 1 \Big/ (C_1 + C_2) \sim 1 \Big/ \sqrt{2\Omega}$. It means that, compared with the usual case, it is much easier to fulfill the conditions of confinement induced resonance in the presence of Raman coupling and SOC. For sufficiently large Raman coupling, the experimental observation of confinement induced resonance needs not resort to the usual magnetic Feshbach resonance techniques.

For fixed SOC strength ($\gamma = 1$), we show in Fig. 6 the bound state energies supported by the "closed" channels (the transversely excited modes) and the full Hamiltonian, respectively[22,27]. The confinement induced resonance can also be viewed as a Feshbach resonance as that in the usual case without Raman coupling and SOC. The resonance condition is satisfied when the energy of the bound states in closed channel coincides with the scattering threshold of the ground transverse modes. In the meantime, the difference between the bound state energies in the closed channels and the full Hamiltonian is $2\hbar\omega_\perp$.

However, based on the same reasons as that in the pure one-dimensional case, the large Raman coupling also changes the existing condition of the bound states in the quasi-one dimension. When the Raman coupling satisfies $\Omega \leq 2\gamma$, there always exist the bound states irrespective of the sign of the s-wave scattering length a_s, which is consistent with the usual case[25] (see the green and blue lines in the panel (**a**) of Fig. 6). However, if $\Omega > 2\gamma$, the bound states exist only for sufficiently large $a_\perp/a_s$ (see red lines). As stated before, the reason is that the spin-orbit coupling and the Raman coupling change greatly the effective density of states near the lowest scattering threshold of energy spectrum. The spin-orbit coupling term $\gamma k(\sigma_2^x - \sigma_1^x)$ does not play significant roles near zero momentum. So the states corresponding to the lowest and highest spectrum belong to spin-triplets, while the state in the middle energy branch is the spin-singlet. In addition, we consider the interactions occurring at the spin-singlet channel. So the bound states can be roughly viewed as the spin-singlet bound states which are mainly supported by the middle energy spectrum. Furthermore, the bound states exist below the lowest threshold (the threshold of triplet energy spectrum). So, the binding energy (relative to the middle energy branch) of bound states has to be larger than the differences between the thresholds of the middle and the lowest energy branches. In other words, the large Raman coupling Ω pushes the energy of bound state low by amount of Ω at least. So, for strong Raman coupling, there exist bound states only when the interaction is strong enough. Then the bound states belong to the deeply binding states of the spin-singlet channel. In consequence, the position of confinement induced resonance is also modified accordingly.

The panel (**b**) of Fig. 5 shows the dependence of the resonance position on the variation of the total momentum K. When the Raman coupling $\Omega = 0$, the spin-orbit coupling terms can be removed by a gauge transformation. So the resonance position is not affected by the total momentum K (see the green line in the panel (**b**)). When the Raman coupling $\Omega \neq 0$, the resonance position $a_s/a_\perp$ becomes smaller and smaller with the increase of K. The panel (**b**) of Fig. 6 shows the energy of bound states for $K \neq 0$ in the quasi-one-dimensional system. Similar to the effects of increasing the Raman coupling Ω, the strong total momentum K also modifies the existing condition of bound states in quasi-one dimension. So the increase of total momentum K amounts to the increase of Raman coupling Ω if the Raman coupling $\Omega \neq 0$.

Here we see what roles the confinement and the SOC (Raman coupling) play, respectively. The confinement freezes the transverse degree of atomic motion, and produces a quasi-one-dimensional system. Due to the enhancement of density of states, there is always

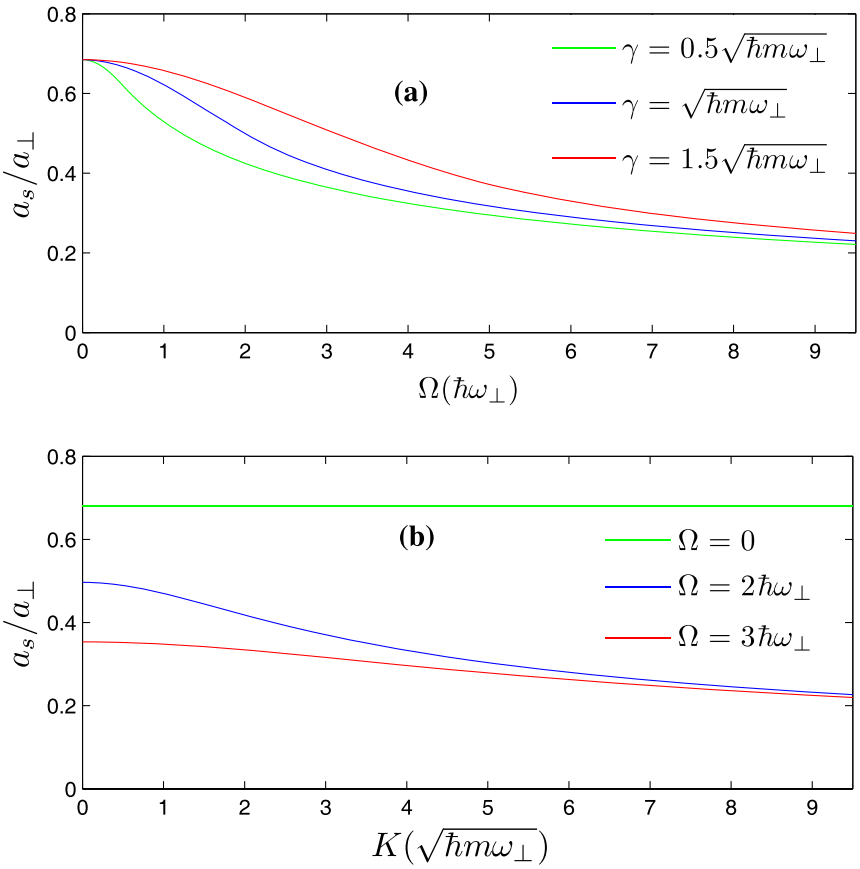

Figure 5 | The resonance position $a_s/a_\perp$ as a function of the Raman parameter Ω and total momentum K ($\gamma = \sqrt{\hbar m\omega_\perp}$). (a): as shown in panel (a) of Fig. 5, when the Raman coupling is absent ($\Omega = 0$) and the incident energy approaches the lowest threshold (the minimum of E_3), the resonance condition is also exactly the same as the case without SOC ($a_s/a_\perp = 1/(C_1 + C_2) = 1/C \approx 0.68$). It is related to the fact that the constant gauge potential can be gauged away by applying a gauge transformation when the Raman coupling is absent. However, in the presence of non-zero Raman coupling, the resonance condition at the lowest threshold could never recover the usual case. (b): the resonance position as a function of total momentum K. For non-vanishing Raman coupling ($\Omega \neq 0$), the resonance position $a_s/a_\perp$ is getting smaller smaller with the increase of the total momentum K.

two-body bound state in the quasi-one-dimensional system no matter how weak the interaction is, as long as the interaction is attractive. After introducing the SOC and Raman coupling, the couplings could reduce, or even change fundamentally the effective density of states near the lowest threshold. The existence condition of bound states is also modified accordingly. The above two competing factors determine the formations of bound states in the confined spin-orbit coupled system.

Discussion

The Raman coupling and SOC have been realized experimentally in ^{40}K atomic gas[38]. Two magnetic sublevels $|\uparrow\rangle = |9/2, 9/2\rangle$ and $|\downarrow\rangle = |9/2, 7/2\rangle$ are chosen as two spin 1/2 states. One can choose the experimental parameters $\gamma/m \sim 2\pi\hbar/(m\lambda) \approx 1.28cm/s$, $\omega_\perp \sim 2\pi \times 17$ kHz with $a_\perp \sim 172\ nm$. The s-wave background scattering length $a_s \sim 170a_0 \sim 9\ nm$. Under the above conditions, the SOC strength $\gamma \sim \sqrt{\hbar m\omega_\perp}$, the ratio $a_s/a_\perp = 0.052$. To satisfy the condition of confinement induced resonance, one can increase Raman coupling strength ($\Omega \sim h \times 3$ MHz) by tuning the intensity of Raman beams. The binding energies of bound states near confinement induced resonance ($E_B \sim 2\hbar w_\perp$) can be measured by using radio-frequency (rf) spectroscopy[52]. It is expected that there are two peaks in the radio-frequency photodissociation spectra. One peak locates at the atomic transition frequency (v_0) of an occupied state to another initially unoccupied state (e.g. $|9/2, 7/2\rangle \rightarrow |9/2, 5/2\rangle$). The other peak at a non-zero detuning ($\delta = v_{rf} - v_0 \sim 34$ kHz) from the atomic transition corresponds to the dissociation of quasi-one-dimensional bound states[25].

In summary, we investigate the effects of SOC and the Raman coupling on the confinement induced resonance. The Raman coupling and spin-orbit coupling fundamentally change the interacting properties of atoms. We propose to realize the confinement induced resonance by increasing Raman coupling strength. Different from the usual way, such as utilizing Feshbach resonances to produce a large scattering length, our work gives a new way to realize the strongly interacting quasi-one-dimensional atomic gas with Raman coupling and spin-orbit coupling. Due to the exotic effects induced by Raman coupling and spin-orbit coupling, a lot of interesting many-body physical phenomena, e.g., the crossover of BCS-BEC superfluidity[53,54], inhomogeneous Fulde-Ferrell-Larkin-Ovhinnikov (FFLO) state[55], fermion pair breaking in the presence of external magnetic field[56], need to be revised in the strong interacting quasi-one dimension atomic gas.

Methods

In this work, we investigate the two-body scattering problem in one-dimensional and the three dimensional cold atomic systems with confinement, respectively. Through comparing the scattering state in the one dimension with that in three dimension, one can get the effective one-dimensional constant (g_{1D}) in terms of the three dimensional s-wave scattering length (a_s).

1 Two-body scattering in one dimension. In this section, we give the detailed calculation of the scattering amplitude. We consider the one-dimensional Hamiltonian of two atoms in the presence of the Raman coupling and the spin-orbit coupling

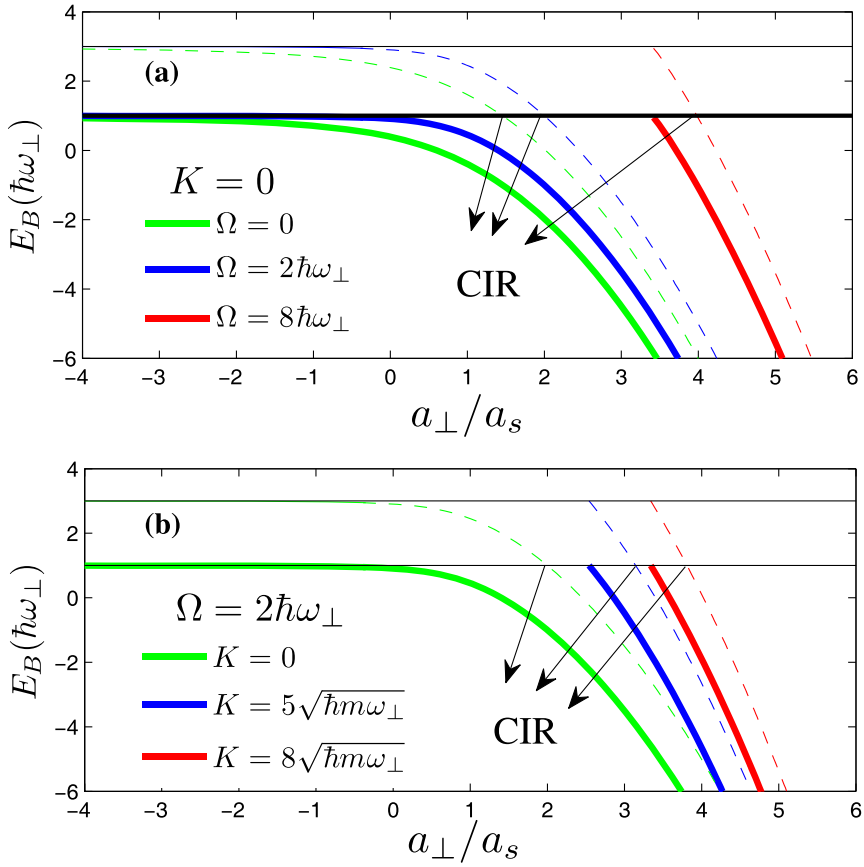

Figure 6 | The bound state energies in the closed channels and the full Hamiltonian, respectively (with SOC strength $\gamma=\sqrt{\hbar m\omega_\perp}$). (a): The bound state energies are measured with respect to the lowest thresholds. The thin lines denote the bound state energies supported by the closed channels, and the thick lines are the bound state energies in the full Hamiltonian. With the increase of Raman coupling Ω, the resonance position $a_s/a_\perp$ (the reciprocal of $a_\perp/a_s$) is getting smaller and smaller, which is consistent with that in panel (a) of Fig. 5. (b): the energy of bound states for various total momentums K. We can see that with the increase of the total momentum K, the modifications of existing conditions of bound states are very similar to that of increasing the Raman coupling. **Note** here the green line in panel (b) corresponds to the blue line in panel (a).

$$H=H_K+H_k,$$

$$H_K=\frac{K^2}{4m}+\frac{\gamma K}{2m}(\sigma_2^x+\sigma_1^x),$$

$$H_k=\frac{k^2}{m}+\frac{\gamma k}{m}\cdot(\sigma_2^x-\sigma_1^x)+\frac{\Omega}{2}(\sigma_2^z+\sigma_1^z)+V.$$

When the total momentum $K=0$, the Hamiltonian of center of mass (H_K) is zero. In the spin basis $\left[(\uparrow\downarrow-\downarrow\uparrow)/\sqrt{2},(\uparrow\uparrow),(\downarrow\downarrow),(\uparrow\downarrow+\downarrow\uparrow)/\sqrt{2}\right]$, the Schrödinger equation in the relative coordinate is

$$[H_0+V(x)]\Psi=E\Psi,$$

$$H_0=\frac{k^2}{m}+M,$$

with

$$M=2\gamma\begin{pmatrix}0&\frac{k}{\sqrt{2}}&-\frac{k}{\sqrt{2}}&0\\ \frac{k}{\sqrt{2}}&\Delta&0&0\\ -\frac{k}{\sqrt{2}}&0&-\Delta&0\\ 0&0&0&0\end{pmatrix}.$$

We introduce $\Delta=\frac{\Omega}{2\gamma}$ in the above equation.

The interaction between atoms can be modeled by zero-range pseudo potential. Therefore the interaction matrix between two atoms takes the form as

$$V(x)=\begin{pmatrix}g_{1D}\delta(x)&0&0&0\\ 0&0&0&0\\ 0&0&0&0\\ 0&0&0&0\end{pmatrix},$$

where g_{1D} is the one-dimensional interaction constant. From the interaction matrix V and matrix M, one can get that the spin channel $(\uparrow\downarrow+\downarrow\uparrow)/\sqrt{2}$ is decoupled from other channels in the case of $K=0$. So we will drop it in the following. The Hamiltonian is reduced a 3×3 matrix. After diagnalizing the H_0, the eigenstates (in coordinate space) and eigenenerges are obtained

$$\Psi_{1,k}(x)=\frac{1}{2\sqrt{(k^2+\Delta^2)}}\begin{pmatrix}-\sqrt{2}k\\ -\left(\sqrt{k^2+\Delta^2}+\Delta\right)\\ \sqrt{k^2+\Delta^2}-\Delta\end{pmatrix}e^{ikx},$$

$$\Psi_{2,k}(x)=\frac{1}{\sqrt{2(k^2+\Delta^2)}}\begin{pmatrix}-\sqrt{2}\Delta\\ k\\ k\end{pmatrix}e^{ikx},$$

$$\Psi_{3,k}(x)=\frac{1}{2\sqrt{(k^2+\Delta^2)}}\begin{pmatrix}\sqrt{2}k\\ -\left(\sqrt{k^2+\Delta^2}-\Delta\right)\\ \sqrt{k^2+\Delta^2}+\Delta\end{pmatrix}e^{ikx},$$

corresponding to eigensnergies $E_1(k)=k^2+2\gamma\sqrt{k^2+\Delta^2}$, $E_2(k)=k^2$, $E_3(k)=k^2-2\gamma\sqrt{k^2+\Delta^2}$, respectively (in the natural units of $m=1, \hbar=1$ and $\gamma=1$). The energy spectrum is shown in panel (**a**) of Fig. 1.

The scattering problem can be solved through the Lipmann-Shwindger equation

$$\Psi(x)=\Psi_0(x)+\int dx' G(\epsilon,x,x')V(x')\Psi(x'),$$

where $G(\epsilon,x,x')=\sum_m\left\langle x\left|\frac{1}{\epsilon-E_m+i\eta}\right|x'\right\rangle$ is the free Green's function. In general, the Green's function is a 3×3 matrix. In the case of zero range interaction the Lipmann-Shwindger equation takes the following form

$$\Psi(x)=\Psi_0(x)+\frac{g_{1D}\Psi_0^1(0)}{1-g_{1D}G_{11}(0)}\begin{pmatrix}G_{11}(x)\\G_{21}(x)\\G_{31}(x)\end{pmatrix}. \quad (4)$$

where $\Psi_0^1(x)$ is the first component of incident state $\Psi_0(x)$ and

$$\begin{aligned}G_{11}(x)=&\frac{1}{2\pi}\int_{-\infty}^{\infty}dk\times e^{ikx}\left[\frac{1}{\epsilon-E_1(k)+i\eta}\frac{k^2}{2(k^2+\Delta^2)}\right.\\&+\frac{1}{\epsilon-E_2(k)+i\eta}\frac{\Delta^2}{k^2+\Delta^2}\\&\left.+\frac{1}{\epsilon-E_3(k)+i\eta}\frac{k^2}{2(k^2+\Delta^2)}\right]\\=&\frac{1}{2\pi}\int_{-\infty}^{\infty}dk\times e^{ikx}\left[\frac{1}{\epsilon-k^2+i\eta}\frac{\Delta^2}{k^2+\Delta^2}\right.\\&\left.+\frac{\epsilon-k^2}{(\epsilon-k^2+i\eta)^2-4\gamma^2(k^2+\Delta^2)}\frac{k^2}{k^2+\Delta^2}\right],\end{aligned}$$

$$\begin{aligned}G_{21}(x)=&\frac{1}{2\pi}\int_{-\infty}^{\infty}dk\times e^{ikx}\left[\frac{1}{\epsilon-E_1(k)+i\eta}\frac{\sqrt{2}k\left(\sqrt{k^2+\Delta^2}+\Delta\right)}{4(k^2+\Delta^2)}+\right.\\&\frac{1}{\epsilon-E_2(k)+i\eta}\frac{-\sqrt{2}k\Delta}{2(k^2+\Delta^2)}+\frac{1}{\epsilon-E_3(k)+i\eta}\\&\left.\frac{-\sqrt{2}k\left(\sqrt{k^2+\Delta^2}-\Delta\right)}{4(k^2+\Delta^2)}\right]\\=&\frac{1}{2\pi}\int_{-\infty}^{\infty}dk\times e^{ikx}\left[\frac{1}{\epsilon-k^2+i\eta}\frac{-\sqrt{2}\Delta k}{2(k^2+\Delta^2)}\right.\\&\left.+\frac{\sqrt{2}[\Delta k(\epsilon-k^2)+2\gamma k(k^2+\Delta^2)]}{(\epsilon-k^2+i\eta)^2-4\gamma^2(k^2+\Delta^2)}\frac{1}{2(k^2+\Delta^2)}\right],\end{aligned}$$

$$\begin{aligned}G_{31}(x)=&\frac{1}{2\pi}\int_{-\infty}^{\infty}dk\times e^{ikx}\left[\frac{1}{\epsilon-E_1(k)+i\eta}\right.\\&\frac{-\sqrt{2}k\left(\sqrt{k^2+\Delta^2}-\Delta\right)}{4(k^2+\Delta^2)}+\frac{1}{\epsilon-E_2(k)+i\eta}\\&\frac{-\sqrt{2}k\Delta}{2(k^2+\Delta^2)}+\frac{1}{\epsilon-E_3(k)+i\eta}\\&\left.\frac{\sqrt{2}k\left(\sqrt{k^2+\Delta^2}+\Delta\right)}{4(k^2+\Delta^2)}\right]\\=&\frac{1}{2\pi}\int_{-\infty}^{\infty}dk\times e^{ikx}\left[\frac{1}{\epsilon-k^2+i\eta}\frac{-\sqrt{2}\Delta k}{2(k^2+\Delta^2)}\right.\\&\left.+\frac{\sqrt{2}[\Delta k(\epsilon-k^2)-2\gamma k(k^2+\Delta^2)]}{(\epsilon-k^2+i\eta)^2-4\gamma^2(k^2+\Delta^2)}\frac{1}{2(k^2+\Delta^2)}\right],\end{aligned}$$

with $\eta\to 0_+$. The above integrals can be obtained by using the residue theorem

$$G_{11}(x)=i\left[\frac{-\Delta^2e^{i\alpha_x|x|}}{2\alpha_2(\alpha_2^2+\Delta^2)}+\frac{(\epsilon-\alpha_1^2)\alpha_1e^{i\alpha_1|x|}}{2(\alpha_1^2-\alpha_3^2)(\alpha_1^2+\Delta^2)}+\frac{(\epsilon-\alpha_3^2)\alpha_3e^{i\alpha_3|x|}}{2(\alpha_3^2-\alpha_1^2)(\alpha_3^2+\Delta^2)}\right],$$

$$\begin{aligned}G_{21}(x)=&i\left[\frac{\sqrt{2}\Delta e^{i\alpha_2|x|}}{4(\alpha_2^2+\Delta^2)}+\frac{\sqrt{2}[\Delta(\epsilon-\alpha_1^2)+2\gamma(\alpha_1^2+\Delta^2)]e^{i\alpha_1|x|}}{4(\alpha_1^2-\alpha_3^2)(\alpha_1^2+\Delta^2)}\right.\\&\left.+\frac{\sqrt{2}[\Delta(\epsilon-\alpha_3^2)+2\gamma(\alpha_3^2+\Delta^2)]e^{i\alpha_3|x|}}{4(\alpha_3^2-\alpha_1^2)(\alpha_3^2+\Delta^2)}\right],\end{aligned}$$

$$\begin{aligned}G_{31}(x)=&i\left[\frac{\sqrt{2}\Delta e^{i\alpha_2|x|}}{4(\alpha_2^2+\Delta^2)}+\frac{\sqrt{2}[\Delta(\epsilon-\alpha_1^2)-2\gamma(\alpha_1^2+\Delta^2)]e^{i\alpha_1|x|}}{4(\alpha_1^2-\alpha_3^2)(\alpha_1^2+\Delta^2)}\right.\\&\left.+\frac{\sqrt{2}[\Delta(\epsilon-\alpha_3^2)-2\gamma(\alpha_3^2+\Delta^2)]e^{i\alpha_3|x|}}{4(\alpha_3^2-\alpha_1^2)(\alpha_3^2+\Delta^2)}\right],\end{aligned}$$

with $\alpha_1=\sqrt{\epsilon+2\gamma^2-2\gamma\sqrt{\epsilon+\gamma^2+\Delta^2}}$, $\alpha_2=\sqrt{\epsilon}$ and $\alpha_3=\sqrt{\epsilon+2\gamma^2+2\gamma\sqrt{\epsilon+\gamma^2+\Delta^2}}$. For $x>0$, the above equations is expressed in another form

$$\begin{pmatrix}G_{11}(x)\\G_{21}(x)\\G_{31}(x)\end{pmatrix}=f_1\Psi_{1,\alpha_1}(x)+f_2\Psi_{2,\alpha_2}(x)+f_3\Psi_{3,\alpha_3}(x),$$

where $f_1=\frac{i\sqrt{2}\gamma}{\alpha_3^2-\alpha_1^2}$, $f_2=\frac{i\Delta}{2\alpha_2\sqrt{\alpha_2^2+\Delta^2}}$, $f_3=\frac{-i\sqrt{2}\gamma}{\alpha_3^2-\alpha_1^2}$. For a given incident energy, there is possibility that there exist several states scattering each other (see Fig. 1). From the Eq. (4), we can explicitly obtain the scattering amplitude for a given incident state. The scattering amplitude makes up to a scattering matrix of rank 1, it can be reduced to one single total amplitude f by diagnalizing the scattering matrix. According to the number of the scattering states, there are several distinct cases.

The incident energy is above the highest scattering threshold $\Omega<\epsilon$ [within energy interval C (see Fig. 1)]. When incident energy satisfies $\Omega<\epsilon$, there will be three eigen-states scattering each other forwardly (all α_1, α_2 and α_3 are real number), which locate at the right semi-axis of relative momentum ($k>0$) (see Fig. 1). The resulting total scattering amplitude is

$$f=\frac{g_{1D}\left[\Psi_{1,\alpha_1}^1(0)f_1+\Psi_{2,\alpha_2}^1(0)f_2+\Psi_{3,\alpha_3}^1(0)f_3\right]}{1-g_{1D}G_{11}(0)}.$$

The incident energy is above the zero-energy, but below the highest threshold Ω ($0<\epsilon<\Omega$ within energy interval B). When incident energy lies in $0<\epsilon<\Omega$, the scattering state on the highest branch is closed (α_1 becomes imaginary number). The remainder two eigen-states scattered each other forwardly. The scattering amplitude is

$$f=\frac{g_{1D}\left[\Psi_{2,\alpha_2}^1(0)f_2+\Psi_{3,\alpha_3}^1(0)f_3\right]}{1-g_{1D}G_{11}(0)}.$$

The scattering energy satisfies $-\Omega<\epsilon<0$ (within energy interval A). When the scattering energy ε lies in the regime $-\Omega<\epsilon<0$, there is only one scattering state on the lowest energy branch (both α_1 and α_2 become imaginary number). The scattering amplitude is

$$f=\frac{g_{1D}\left[\Psi_{3,\alpha_3}^1(0)f_3\right]}{1-g_{1D}G_{11}(0)}.$$

2 The confinement induced resonance. The scattering problem in three dimension with confinement can be solved as follow. We assume the confinement is strong enough that only the transverse harmonic ground state is occupied. The incident energy with respect to the lowest threshold and the ground state energy of transverse harmonic oscillator should be lower than the transverse exited state energy. The lowest excited state which can be coupled to ground states by the s-wave interaction is $\phi_1(y)\phi_1(z)$ with energy $2\hbar\omega_\perp$[22,57]. Then, the incident energy of scattering states should $\epsilon<2\hbar\omega_\perp=2$ (in natural units of $m=1$, $\hbar=1$ and $\omega_\perp=1$). Using the Lipmann-Shwindger equation, three dimension scattering wave function can be obtained

$$\Psi(r)_{3D}=\phi_0(y)\phi_0(z)\Psi_0(x)+\int dr' G_{3D}(\epsilon,r,r')V(r')\Psi_{3D}(r'),$$

where $\phi_n(t)=\left(\sqrt{\pi}2^n n!a_\perp\right)^{-1/2}e^{-t^2/2a_\perp^2}H_n(t/a_\perp)$, $a_\perp=\sqrt{\frac{\hbar}{\mu\omega_\perp}}=\sqrt{2}$ is wave

function and the length scale of transverse Harmonic oscillator. $\Psi_0(x)$ is one dimensional incident wave function along x direction as above section. The interaction V is the pseudo-potential $V(r)=|s\rangle\langle s|\otimes\frac{4\pi\hbar^2 a_s}{m}\delta(\vec{r})\partial_r(r\cdot)$. Substituting the interaction V, the wave function in three dimension becomes

$$\Psi_{3D}(x,y,z)=\phi_0(y)\phi_0(z)\Psi_0(x)+g_{3D}F\begin{pmatrix}(G_{3D}(r))_{11}\\(G_{3D}(r))_{21}\\(G_{3D}(r))_{31}\end{pmatrix},$$

where $F=lim_{r\to 0}\partial_r\left[r\left(\Psi^1_{3D}(r)\right]\right.$, $\Psi^1_{3D}(r)$ is first component of three dimensional wave function. Focusing on $y = z = 0$ and the resulting qusi-one dimensional wave function is

$$\begin{aligned}\Psi(x)&=\frac{\Psi_{3D}(x,0,0)}{\phi_0(0)\phi_0(0)}\\&=\Psi_0(x)+\frac{g_{3D}\Psi^1_0(0)}{1-g_{3D}\left(G_{3d}(0)_{11}\right)_r}\begin{pmatrix}(G_{3D}(x,0,0))_{11}\\(G_{3D}(x,0,0))_{21}\\(G_{3D}(x,0,0))_{31}\end{pmatrix},\end{aligned}\tag{5}$$

where $(G_{3D}(0)_{11})_r = lim_{r\to 0}\partial_r[r(G_{3D}(r)_{11})]$ is the regular part of the Green's function matrix element G_{11} at origin. It is known that when $r \to 0$, the three dimensional Green's function in confined system also diverges as that in homogeneous space $(G_{3D}(r)_{11})_{r\to 0} \propto -1/4\pi r$[58]. In order to obtain the regular part, we need to subtract the singular part $(-1/4\pi r)$ from $G_{3D}(r)_{11}$ near the origin. For the qusi-one dimensional scattering problem, we only need to know the long-ranged asymptotic behavior of three dimensional Green's function and the regular part of $G_{3D}(x, y = 0, z = 0)_{11}$ near $x = 0$. The Green's function can be decomposed as two terms:

$$\begin{aligned}G_{3D}(\epsilon,x,y=0,z=0)&=\left\langle x,0,0\left|\frac{1}{\epsilon-H_0+H_\perp+i\eta}\right|0,0,0\right\rangle\\&=\sum_{n_1,n_2,k,m}\frac{\phi^*_{n_1}(0)\phi^*_{n_2}(0)\phi_{n_1}(0)\phi_{n_2}(0)\langle x\mid\Psi_{m,k}\rangle\langle\Psi_{m,k}\mid 0\rangle}{\epsilon-[n_1+n_2+1-E_m(k)]+i\eta}\\&=G_{3D1}+G_{3D2},\end{aligned}$$

where

$$G_{3D1}=\sum_{k,m}\frac{\phi^*_0(0)\phi^*_0(0)\phi_0(0)\phi_0(0)\langle x\mid\Psi_{m,k}\rangle\langle\Psi_{m,k}\mid 0\rangle}{\epsilon-[1-E_m(k)]+i\eta},$$

and

$$\begin{aligned}G_{3D2}=-\sum_{[n_1,n_2,k,m]'}\int_0^\infty dt e^{-[n_1+n_2+1-E_m(k)-\epsilon]t}\\\left[\phi^*_{n_1}(0),\phi^*_{n_2}(0)\phi_{n_1}(0)\phi_{n_2}(0)\langle x\mid\Psi_{m,k}\rangle\langle\Psi_{m,k}\mid 0\rangle\right],\end{aligned}$$

here $|\Psi_{m,k}\rangle$ are the eigenstates of H_0 which is same as that in the above section. The summation $\sum_{[n_1,n_2k,m]'}$ excludes the term $[n_1 = 0, n_2 = 0, k, m]$, the identity $\frac{1}{n}=\int_0^\infty dte^{-nt}(n>0)$ has been used in the above Equation. The first part G_{3D1} is related to the scattering channel and long ranged, while the second part G_{3D2} is short ranged corresponding to influences of virtual transition of other closed channels. Redefining the reference point of energy $\epsilon\to\epsilon-1$, it is easy to see that the first term G_{3D1} is just the one dimensional Green's function $G(x)$ up to a factor $|\phi_0(0)|^4 = 1/2\pi$. In the following, we will see the short-ranged part of matrix element $(G_{3D2}(x))_{11}$ is related to confinement induced resonance (CIR).

Using $\sum_{n=0}^\infty\frac{\left(\frac{t}{2}\right)^n}{n!}H_n(x)H_n(y)=\left(1-t^2\right)^{-1/2}exp\left[\frac{2xyt-(x^2+y^2)t^2}{1-t^2}\right]$, completing the summation over the index $[n_1, n_2]$, the second part of the matrix element $(G_{3D2}(x))_{11}$ takes the form

$$\begin{aligned}(G_{3D2}(x))_{11}&=-\frac{1}{8\pi^2}\int_0^\infty dt\frac{e^{\epsilon t/2}}{e^t-1}\int_{-\infty}^\infty dke^{-k^2t/2+ikx}\\&\left[\frac{\Delta^2}{k^2+\Delta^2}+cosh\left[\gamma t\sqrt{k^2+\Delta^2}\right]\frac{k^2}{k^2+\Delta^2}\right]\\&=\chi_1+\chi_2,\end{aligned}$$

where

$$\chi_1(x)=-\frac{1}{8\pi^2}\int_0^\infty dt\frac{e^{\epsilon t/2}}{e^t-1}\int_{-\infty}^\infty dke^{-k^2t/2+ikx},$$

and

$$\begin{aligned}\chi_2(x)=-\frac{1}{8\pi^2}\int_0^\infty dt\frac{e^{\epsilon t/2}}{e^t-1}\int_{-\infty}^\infty dke^{-k^2t/2+ikx}\\\left[cosh\left[\gamma t\sqrt{k^2+\Delta^2}\right]-1\right]\frac{k^2}{k^2+\Delta^2}.\end{aligned}$$

It can be shown that the $\chi_2(x)$ is not singular as $x \to 0$, while the $\chi_1(x)$ does diverge $\chi_1(x) \propto -1/4\pi x$. Substracting the diverging part,

$$\chi_{1r}(0)=-\frac{\sqrt{2\pi}}{8\pi^2}\int_0^\infty dt\left[\frac{e^{\epsilon t/2}}{(e^t-1)\sqrt{t}}-\frac{1}{t^{3/2}}\right].$$

So the regular part of Green's function $(G_{3D}(0)_{11})_r = G_{11}(0)|\phi(0)|^4 + \chi_{1r}(0) + \chi_2(0)$. For $x\gg 1$, the Green's function $G_{3D}(x\gg 1,0,0)\approx G_{3D1}(x,0,0)=|\phi_0(0)|^4G(x)$, $G(x)$ is the Green's function in pure one domension. Comparing Eq. (4) with (5), we can get the one-dimensional effective interaction constant in term of the three dimensional s-wave interaction constant

$$g_{1D}=\frac{g_{3D}/2\pi}{1-g_{3D}(\chi_{1r}(0)+\chi_2(0))}.$$

Introducing $\chi_{1r}(0)=\sqrt{2}C_1\Big/8\pi$, $\chi_2(0)=\sqrt{2}C_2\Big/8\pi$ and using $g_{3D}=\frac{4\hbar^2\pi a_s}{m}$, $a_\perp=\sqrt{2}$, $m = 2\mu$ and $\Delta=\frac{\Omega}{2\gamma}$, the above equation is reduced to Eq. (3) in the main text.

$$g_{1D}=\frac{2\hbar^2a_s}{\mu a_\perp^2}\frac{1}{1-(C_1+C_2)a_s/a_\perp},$$

with

$$\begin{aligned}C_1&=\frac{-1}{\sqrt{\pi}}\int_0^\infty dt\left[\frac{e^{\epsilon t/2}}{(e^t-1)\sqrt{t}}-\frac{1}{t^{3/2}}\right],\\C_2&=\frac{-1}{\sqrt{2\pi}}\int_0^\infty dt\frac{e^{\epsilon t/2}}{e^t-1}\int_{-\infty}^\infty dke^{-k^2t/2}\\&\left[cosh\left[\gamma t\sqrt{k^2+(\Omega/2\gamma)^2}\right]-1\right]\frac{k^2}{k^2+(\Omega/2\gamma)^2}.\end{aligned}$$

1. Wu, C. J., Shem, I. M. & Zhou, X. F. Unconventional Bose-Einstein Condensations from Spin-Orbit Coupling. *Chin. Phys. Lett.* **28**, 097102 (2011).
2. Wang, C., Cao, C., Jian, C. M. & Zhai, H. Spin-Orbit Coupled Spinor Bose-Einstein Condensates. *Phys. Rev. Lett.* **105**, 160403 (2010).
3. Ho, T. L. & Zhang, S. Bose-Einstein Condensates with Spin-Orbit Interaction. *Phys. Rev. Lett.* **107**, 150403 (2011).
4. Yip, S. K. Bose-Einstein condensation in the presence of artificial spin-orbit interaction. *Phys. Rev. A* **83**, 043616 (2011).
5. Hu, H., Ramachandhran, B., Pu, H. & Liu, X. J. Spin-Orbit Coupled Weakly Interacting Bose-Einstein Condensates in Harmonic Traps. *Phys. Rev. Lett.* **108**, 010402 (2012).
6. Sinha, S., Nath, R. & Santos, L. Trapped Two-Dimensional Condensates with Synthetic Spin-Orbit Coupling. *Phys. Rev. Lett.* **107**, 270401 (2011).
7. Zhou, X. F., Zhou, J. & Wu, C. J. Vortex structures of rotating spin-orbit-coupled Bose-Einstein condensates. *Phys. Rev. A* **84**, 063624 (2011).
8. Su, S. W. *et al.* Crystallized half-skyrmions and inverted half-skyrmions in the condensation of spin-1 Bose gases with spin-orbit coupling. *Phys. Rev. A* **86**, 023601 (2012).
9. Liu, C. F. *et al.* Circular-hyperbolic skyrmion in rotating pseudo-spin-1/2 Bose-Einstein condensates with spin-orbit coupling. *Phys. Rev. A* **86**, 053616 (2012).
10. Zhou, X., Li, Y., Cai, Z. & Wu, C. Unconventional states of bosons with the synthetic spin-orbit coupling. *J. Phys. B: At. Mol. Opt. Phys.* **46**, 134001 (2013).
11. Vyasanakere, J. P. & Shenoy, V. B. Bound states of two spin–1/2 fermions in a synthetic non-Abelian gauge field. *Phys. Rev. B* **83**, 094515 (2011).
12. Yu, Z. Q. & Zhai, H. Spin-Orbit Coupled Fermi Gases across a Feshbach Resonance. *Phys. Rev. Lett.* **107**, 195305 (2011).
13. Liao, R. Y., Yu, Y. X & Liu, W. M. Tuning the Tricritical Point with Spin-Orbit Coupling in Polarized Fermionic Condensates. *Phys. Rev. Lett.* **108**, 080406 (2012).
14. Vaishnav, J. Y. & Clark, C. W. Observing Zitterbewegung with Ultracold Atoms. *Phys. Rev. Lett.* **100**, 153002 (2008).
15. Zhang, Y. C., Song, S. W., Liu, C. F. & Liu, W. M. *Zitterbewegung* effect in spin-orbit-coupled spin-1 ultracold atoms. *Phys. Rev. A* **87**, 023612 (2013).
16. Cui, X. Mixed-partial-wave scattering with spin-orbit coupling and validity of pseudopotentials. *Phys. Rev. A* **85**, 022705 (2012).
17. Zhang, P., Zhang, L. & Deng, Y. Modified Bethe-Peierls boundary condition for ultracold atoms with spin-orbit coupling. *Phys. Rev. A* **86**, 053608 (2012).

18. Wu, Y. & Yu, Z. Short-range asymptotic behavior of the wave functions of interacting spin-1/2 fermionic atoms with spin-orbit coupling: A model study. *Phys. Rev. A* **87**, 032703 (2013).
19. Zhang, L., Deng, Y. & Zhang, P. Scattering and effective interactions of ultracold atoms with spin-orbit coupling. *Phys. Rev. A* **87**, 053626 (2013).
20. Zhang, P., Zhang, L. & Zhang, W. Interatomic collisions in two-dimensional and quasi-two-dimensional confinements with spin-orbit coupling. *Phys. Rev. A* **86**, 042707 (2012).
21. Olshanii, M. Atomic Scattering in the Presence of an External Confinement and a Gas of Impenetrable Bosons. *Phys. Rev. Lett.* **81**, 938 (1998).
22. Bergeman, T., Moore, M. G. & Olshanii, M. Atom-Atom Scattering under Cylindrical Harmonic Confinement: Numerical and Analytic Studies of the Confinement Induced Resonance. *Phys. Rev. Lett.* **91**, 163201 (2003).
23. Petrov, D. S., Holzmann, M. & Shlyapnikov, G. V. Bose-Einstein Condensation in Quasi-2D Trapped Gases. *Phys. Rev. Lett.* **84**, 2551 (2000).
24. Petrov, D. S. & Shlyapnikov, G. V. Interatomic collisions in a tightly confined Bose gas. *Phys. Rev. A* **64**, 012706 (2001).
25. Moritz, H. *et al.* Confinement Induced Molecules in a 1D Fermi Gas. *Phys. Rev. Lett.* **94**, 210401 (2005).
26. Haller, E. *et al.* Confinement-Induced Resonances in Low-Dimensional Quantum Systems. *Phys. Rev. Lett.* **104**, 153203 (2010).
27. Peng, S. G. *et al.* Confinement-induced resonance in quasi-one-dimensional systems under transversely anisotropic confinement. *Phys. Rev. A* **82**, 063633 (2010).
28. Zhang, W. & Zhang, P. Confinement-induced resonances in quasi-one-dimensional traps with transverse anisotropy. *Phys. Rev. A* **83**, 053615 (2011).
29. Kinoshita, T.,Wenger, T. & Weiss, D. S. Observation of a One-Dimensional Tonks-Girardeau Gas. *Science* **305**, 1125 (2004).
30. Paredes, B. *et al.* Tonks-Girardeau gas of ultracold atoms in an optical lattice. *Nature* **429**, 277 (2004).
31. Recati, A., Fedichev, P. O., Zwerger, W. & Zoller, P. Spin-Charge Separation in Ultracold Quantum Gases. *Phys. Rev. Lett.* **90**, 020401 (2003).
32. Kakashvili, P., Bhongale, S. G., Pu, H. & Bolech, C. J. Realizing Luttinger liquids in trapped ultra-cold atomic Fermi gases using 2D optical lattices. *Physica B* **404**, 3320 (2009).
33. Hu, H., Jiang, L., Pu, H., Chen, Y. & Liu, X. J. Universal Impurity-Induced Bound State in Topological Superfluids. *Phys. Rev. Lett.* **110**, 020401 (2013).
34. Sato, M., Takahashi, Y. & Fujimoto, S. Non-Abelian Topological Order in s-Wave Superfluids of Ultracold Fermionic Atoms. *Phys. Rev. Lett.* **103**, 020401 (2009).
35. Wu, F., Guo, G. C., Zhang, W. & Yi, W. Unconventional Superfluid in a Two-Dimensional Fermi gas with Anisotropic Spin-Orbit Coupling and Zeeman fields. *Phys. Rev. Lett.* **110**, 110401 (2013).
36. Lin, Y. J., García, K. J. & Spielman, I. B. Spin-orbit-coupled Bose-Einstein condensates. *Nature* **471**, 83 (2011).
37. Lin, Y. J. *et al.* Bose-Einstein Condensate in a Uniform Light-Induced Vector Potential. *Phys. Rev. Lett.* **102**, 130401 (2009).
38. Wang, P. J. *et al.* Spin-Orbit Coupled Degenerate Fermi Gases. *Phys. Rev. Lett.* **109**, 095301 (2012).
39. Cheuk, L. W. *et al.* Spin-Injection Spectroscopy of a Spin-Orbit Coupled Fermi Gas. *Phys. Rev. Lett.* **109**, 095302 (2012).
40. Dalibard, J., Gerbier, F., Juzeliūnas, G. & Öhberg, P. Colloquium: Artificial gauge potentials for neutral atoms. *Rev. Mod. Phys.* **83**, 1523 (2011).
41. Olson, A. J. *et al.* Tunable Landau-Zener transitions in a spin-orbit coupled Bose-Einstein condensate. arXiv: 1310.1818v1 (2013).
42. Liu, X. J. Impurity probe of topological superfluids in one-dimensional spin-orbit-coupled atomic Fermi gases. *Phys. Rev. A* **87**, 013622 (2013).
43. Wei, R. & Mueller, E. J. Majorana fermions in one-dimensional spin-orbit-coupled Fermi gases. *Phys. Rev. A* **86**, 063604 (2012).
44. Taylor, J. R. Scattering Theory (Wiley, New York, 1972).
45. Saeidian, S., Melezhik, V. S. & Schmelcher, P. Multichannel atomic scattering and confinement-induced resonances in waveguides. *Phys. Rev. A* **77**, 042721 (2008).
46. Duine, R. A. & Stoof, H. T. C. Atom-molecule coherence in Bose gases. *Physics Reports* **396**, 115 (2004).
47. Köhler, T., Góral, K. & Julienne, P. Production of cold molecules via magnetically tunable Feshbach resonances. *Rev. Mod. Phys.* **78**, 1311 (2006).
48. Chin, C., Grim, R., Julienne, P. & Tiesinga, E. Feshbach resonances in ultracold gases. *Rev. Mod. Phys.* **82**, 1225 (2010).
49. Celi, A. *et al.* Synthetic gauge fields in synthetic dimensions. *Phys. Rev. Lett.* **112**, 043001 (2014).
50. Huang, K. & Yang, C. N. Quantum-Mechanical Many-Body Problem with Hard-Sphere Interaction. *Phys. Rev.* **105**, 767 (1957).
51. Huang, K. Statistical Mechanics (Wiley, New York, 1987).
52. Regal, C. A., Ticknor, C., Bohn, J. L. & Jin, D. S. Creation of ultracold molecules from a Fermi gas of atoms. *Nature* **424**, 47 (2003).
53. Fuchs, J. N., Recati, A. & Zwerger, W. Exactly Solvable Model of the BCS-BEC Crossover. *Phys. Rev. Lett.* **93**, 090408 (2004).
54. Tokatly, I. V. Dilute Fermi Gas in Quasi-One-Dimensional Traps: From Weakly Interacting Fermions via Hard Core Bosons to a Weakly Interacting Bose Gas. *Phys. Rev. Lett.* **93**, 090405 (2004).
55. Hu, H., Liu, X. J. & Drummond, P. D. Phase Diagram of a Strongly Interacting Polarized Fermi Gas in One Dimension. *Phys. Rev. Lett.* **98**, 070403 (2007).
56. Guan, X. W., Batchelor, M. T., Lee, C. & Bortz, M. Phase transitions and pairing signature in strongly attractive Fermi atomic gases. *Phys. Rev. B* **76**, 085120 (2007).
57. Busch, T., Englert, Be. G., Rzążewski, K. & Wilkens, M. Two Cold Atoms in a Harmonic Trap. *Found. Phys.* **28**, 549 (1998).
58. Idziaszek, Z. & Calarco, T. Analytical solutions for the dynamics of two trapped interacting ultracold atoms. *Phys. Rev. A* **74**, 022712 (2006).

Acknowledgments

Yi-Cai Zhang thank Lin Wen, Fadi Sun, Fei Zhou, Ran Qi, Daw-Wei Wang and Xiaolin Cui for useful discussion. This work was supported by the NKBRSFC under grants Nos. 2011CB921502, 2012CB821305, NSFC under grants Nos. 61227902, 61378017, 11311120053.

Author contributions

Y.C.Z. performed calculations. Y.C.Z., S.S.W., W.M.L. analyzed numerical results. Y.C.Z., S.S.W., W.M.L. contributed in completing the paper.

Additional information

Competing financial interests: The authors declare no competing financial interests.

How to cite this article: Zhang, Y.-C., Song, S.-W. & Liu, W.-M. The confinement induced resonance in spin-orbit coupled cold atoms with Raman coupling. *Sci. Rep.* **4**, 4992; DOI:10.1038/srep04992 (2014).